Nano Research
DOI 10.1007/s12274-015-0749-3
Research Article
ISSN 1998-0124
CN 11-5974/O4

Influence of external electric field on piezotronic effect in ZnO nanowires

Fei Xue[1], Limin Zhang[1], Xiaolong Feng[1], Guofeng Hu[1], Feng Ru Fan[1], Xiaonan Wen[2], Li Zheng[2] and Zhong Lin Wang[1,2] (✉)

[1] *Beijing Institute of Nanoenergy and Nanosystems, Chinese Academy of Sciences, Beijing, 100083, China*
[2] *School of Material Science and Engineering, Georgia Institute of Technology, Atlanta, Georgia 30332, USA*

Received: 16 November 2014
Revised: 3 February 2015
Accepted: 16 February 2015

KEYWORDS
piezotronic effect,
external electric field,
ZnO nanowires

ABSTRACT

In this work, the piezotronic effect is investigated for the first time in external electric fields ranging from 0 V·cm^{-1} to 2,000 V·cm^{-1} by using n-type ZnO nanowires supported by a flexible substrate. In the presence of an external electric field, the Schottky barrier height (SBH) is lowered by the image force, allowing more free carriers to pass through the metal-semiconductor junction and enhancing the screening effect on positive piezoelectric polarization charges. As the strength of the external electric field increases, the piezotronic effect is significantly suppressed and the metal-semiconductor contact finally exhibits Ohmic behavior. The experimental results show that devices can be classified into three groups, corresponding to low, moderate, and high carrier densities of the nanowires used. This work not only helps us to explicate the basic physical mechanism of the piezotronic effect in a harsh environment in an electric field but also provides guidelines for future design and fabrication of piezotronic devices.

1 Introduction

Wurtzite and zinc blende structured materials, such as ZnO, ZnS, GaN, CdS, and CdSe, have significant potential in novel applications owing to their conjunction of piezoelectric and semiconductor properties. The piezoelectric potential (piezopotential) created in a crystal under strain acts as a "gate" for modulating the transport of carriers across the p-n junction and metal-semiconductor interface. This novel mechanism for influencing the transport characteristics was first proposed as a piezotronic effect in 2007 [1, 2]. A number of high-performance devices have been fabricated based on this effect, such as strain sensors [3, 4], piezopotential gated transistors [5, 6], LEDs [7], solar cells [8], photodetectors [9], and temperature sensors [10]. Meanwhile, in-depth and systematic experimental and theoretical studies of this effect have been conducted [11–16], leading us to a better understanding of this physical phenomenon. However, up to now,

Address correspondence to Zhong Lin Wang, zlwang@gatech.edu

no relevant research has been conducted to explore the basics of the piezotronic effect in the presence of electric fields. Taking into account the complex and varying ambient conditions that may be experienced by the devices, investigating the impact of external electric fields on the piezotronic effect is of importance not only for clearly explicating this effect, but also for developing novel and functional piezotronic devices.

In this work, as-synthesized ultra-long ZnO nanowires were transferred to a flexible substrate for fabricating piezotronic devices, while silver paste was chosen as the material for metal electrodes. Over 40 devices were characterized for the piezotronic measurement in electric fields ranging from 0 V·cm^{-1} to 2,000 V·cm^{-1}. Devices were categorized into three groups according to the doping levels of the nanowires used, namely the groups corresponding to low, moderate, and high carrier densities. When the intensity of the external electric field was increased, the Schottky barrier height (SBH) was gradually lowered by the image-force and eventually the devices exhibited Ohmic contact behavior. Moreover, the piezotronic response was more suppressed with increasing intensity of the electric field. This was ascribed to the enhanced screening effect on positive piezoelectric polarization charges from the free carriers.

2 Experimental section

Ultra-long ZnO nanowires used in this work were synthesized by using vapor-solid growth process as described previously [17, 18]. The nanowires were 200–300 μm long and around 3 μm in diameter. To fabricate the device, the chosen nanowires were picked up and transferred onto the center of a flexible polyethylene terephthalate (PET) substrate (0.5 cm × 3 cm, 600-μm-thick) with the axis of the nanowire kept parallel to the substrate's long edge. Silver paste was used for fixing both ends of the nanowire on the substrate and for forming electrical contacts, creating a metal-semiconductor-metal (M-S-M) structure. A typical optical image of an as-fabricated device is shown in Fig. 1(a). The two ends of a nanowire were defined as source and drain, respectively. The experimental setup is shown in Fig. 1(b). One end of the device was fastened to a bracket (PMMA) and the other end was free. Tensile strain was introduced by a positioner, which was driven by a three-dimensional stage with a 1-μm-resolution. A capacitor of a pair of parallel metal aluminum plates (4 cm × 4 cm, 500-μm-thick) was used for providing varying electric field by connecting to a DC voltage source. Electrical measurements of the device were performed in electric fields ranging from 0 V·cm^{-1} to 2,000 V·cm^{-1}. The dielectric medium in this equipment, such as the substrate (PET), changed the external electric field's direction as shown in Fig. 1(b).

3 Results and discussion

The effect of external electric field on the metal-semiconductor system is illustrated in Fig. 2. Here, for simplicity we assumed that the direction of the external electric field is along the negative x axis. When the metal-semiconductor system is exposed to an external electric field, an electron at a distance of x

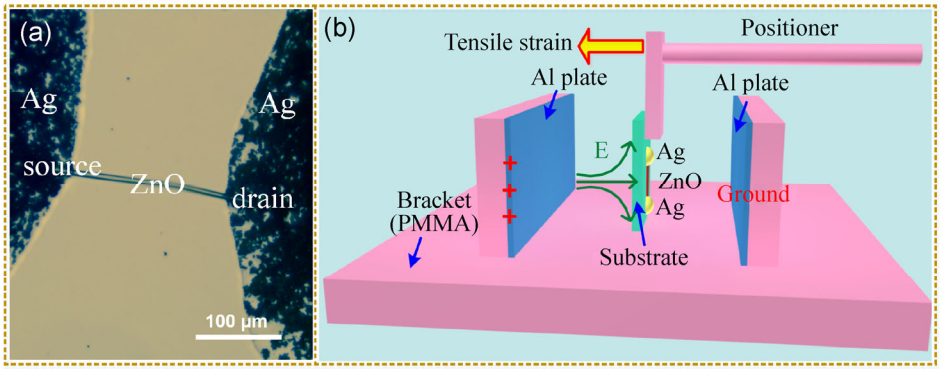

Figure 1 (a) Optical microscopy image of a typical ZnO nanowire device. (b) Schematic of the measurement set-up for studying the piezotronic effect in a ZnO nanowire.

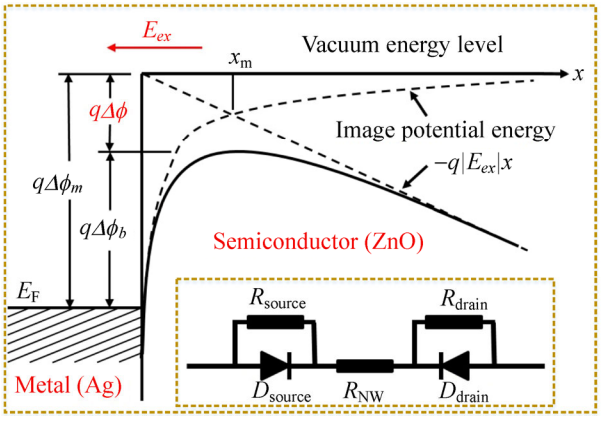

Figure 2 Energy band diagram illustrating the influence of external electric field on the SBH. The external electric field was assumed to be along the negative x axis. The intrinsic barrier height is $q\Delta\phi_m$, the effective barrier height is $q\Delta\phi_b$, and the electric potential energy of an electron is $-q|E_{ex}|x$. The lowering barrier height is $q\Delta\phi$, due to the addition of image potential energy and electric potential energy in the presence of the external electric field. The inset is the equivalent circuit diagram of a typical MSM model used in this work.

from the metal surface induces a positive charge on the metal surface. The Coulomb force between the electron and the induced positive charge is equivalent to the force that would exist between the electron and an equal positive charge located at $-x$. This positive charge is referred to as the image charge and the force of attraction toward the metal is called the image force. The image potential energy of an electron coupled with the electric potential energy lowers the SBH in the presence of an external electric field, and the altered barrier height is given by Eq. (1) [19]:

$$\Delta\phi = \sqrt{\frac{q|E_{ex}|}{4\pi\varepsilon_s}} \quad (1)$$

in which E_{ex} is the strength of the external electric field and ε_s is the semiconductor's permittivity. However, external electric fields in other directions, not parallel to the x axis, will also result in the lowered SBH [19]. An MSM model is applied for performing the quantitative analysis of the experimental data for obtaining the relevant parameters for a device, such as the conductivity and SBH. The inset in Fig. 2(a) shows an equivalent circuit for the MSM model. Before characterizing the three groups of devices with Schottky contact, ten devices with Ohmic contact were measured for studying whether the electrons' density and drift velocity vary under different intensities of the external electric field. I–V curves exhibit no distinct changes as shown in Fig. S1. On the one hand, in the external electric field the carriers in the nanowires are speeded up; on the other hand, their movements are blocked by strong lattice scattering [19]. According to Eq. (2) [19], under this experimental condition, the density of electrons multiplied by the electron mobility is nearly constant for different intensities of the external electric field. The electrons acquire energy from the external electric field and lose most of this energy to phonons. Hence, the electrons that are speeded up by the external electric field insignificantly affect the change in the electrical properties, which can help us to better understand the carrier transport in the MSM model:

$$J = \sigma E_{bias} = qn\mu E_{bias} \quad (2)$$

where J is the current density, σ is the conductivity, n is the density of electrons in ZnO, μ is the mobility of the carriers, and E_{bias} is the electric field's strength of the bias voltage applied to the ZnO semiconductor. In terms of the piezotronic response characteristics, the Schottky-contact devices can be divided into three groups according to the carrier density in the nanowires, namely the low, moderate, and high carrier density.

The responses of the first group of devices with low carrier density, about $6 \times 10^{17}/\text{cm}^3$, are shown in Figs. 3(a) to 3(c) for different intensities of the external electric field. The devices exhibited typical non-linear and non-symmetrical I–V curves, demonstrating that the SBHs at the two contacts are different. In the MSM model, two back-to-back diodes are proposed to replace the two Schottky barriers. The transport properties are dominantly controlled by the reversely biased Schottky barrier under positive or negative bias voltage. The strain in the nanowire is estimated by using the previously demonstrated method [3, 5]. In practice, when an external tensile strain is applied to a device, there will be strain components parallel and normal to the nanowires axis, yielding a non-uniform spatial distribution of piezopotential. Such a result can possibly affect the piezotronic devices' performance. In general, the Ag electrode is in

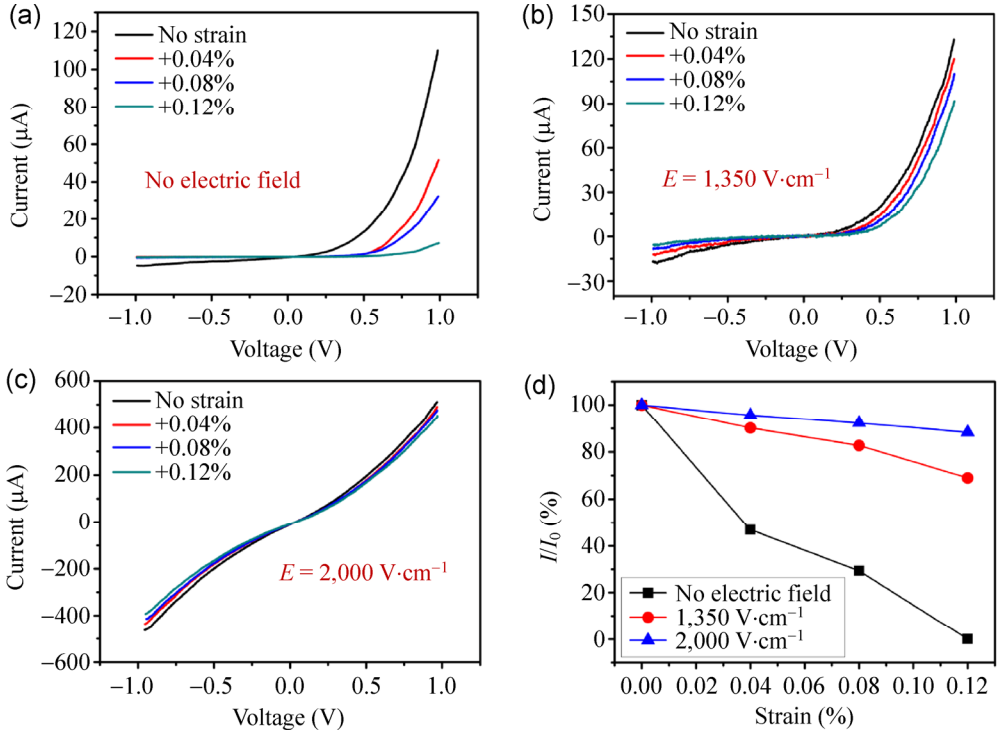

Figure 3 *I–V* curves of a low-conductivity device. Typical change in transport characteristics with applied strains for electric field intensities of (a) 0 V·cm^{-1}, (b) 1,350 V·cm^{-1}, (c) 2,000 V·cm^{-1}. (d) Relative changes in the current at the source electrode, for different applied strains and external electric field intensities, demonstrating that the piezotronic effect is suppressed with increasing external electric field's intensity.

contact with three types of crystalline planes of the ZnO nanowire: top electrode configuration, bottom electrode configuration and fully enclosed electrode configuration [20]. For this work, the electrical contact between the ZnO nanowire and the Ag electrode was the bottom electrode configuration. The piezopotential in the contact area between the substrate and the two ends of the ZnO nanowire increases with increasing vertical strain component, and the SBHs at the two strained electrodes are linearly related, positive, but have different magnitudes. When the applied tensile strain increases, the current flowing through the device decreases substantially in both the positive and negative voltage ranges. As the intensity of the external electric field is increased, the current in the entire bias voltage range increases as well and the piezotronic response is weakened significantly. When the intensity of the external electric field reaches 2,000 V·cm^{-1}, the *I–V* characteristic presents a nearly straight line, exhibiting the properties of Ohmic contact device. Meanwhile, the varying trends for different tensile strains are further inhibited by the external electric field. This phenomenon is observed here for the first time. Figure 3(d) shows the relative current change at the source electrode, for different applied strains and external electric field's intensities. The varying trend for different applied tensile strains is more remarkable in the absence of the electric field and gradually becomes restrained as the external electric field's intensity increases.

In the above experiment, the nanowire's orientation relative to the external field would also change during the introduction of the strain. Next, without any applied strain, we kept the ZnO nanowire device normal to the electrode plate for observing the behaviors at different electric field intensities, as indicated in Fig. S2. The results agree with the data in Fig. 3. Figure S1 clarifies that the effect of electron acceleration is so weak that it can be ignored. We attribute this phenomenon mainly to the image-force lowering of barrier height, which allows many more free carriers to drift through the metal-semiconductor interface,

enhancing the screening effect on the positive piezoelectric polarization charges. Therefore, the piezopotential of the carrier transport is largely suppressed in the model of the bottom electrode configuration, yielding the reduction in variation of *I*–*V* curves trends with increasing external electric field's intensity. The SBH is the principal factor leading to the restrained piezotronic response; the SBH descent exists irrespective of the external electric field's direction relative to the negative x axis, as depicted in Fig. 2; hence, the external electric field always reduces the piezotronic effect regardless of its direction.

To clearly illustrate the underlying physical mechanism, some relevant parameters were derived from simulating the electric transport properties by using the MSM model [21, 22]. The first principal assumption of this model is that the nanowire is far longer than the carrier's mean free path. Hence, the carrier transport is within the diffusive regime and the nanowire's conductivity in the non-depleted part can be described by Ohm's law [12]. In fact, the nanowires in this work were about 200-μm to 300-μm-long, completely satisfying the above assumption. Second, it is necessary for the nanowire's radius to be much larger than the de Broglie wavelength. Electron-electron and electron-phonon interactions are so weak that they can be ignored, and the effective mass approximation can be used. Third, the doping concentration should be well-distributed throughout the nanowire. Fourth, the contact area at the source electrode should be the same as that at the drain electrode. In the crystal, the drift velocity of the carriers (electrons) sharply increases following the application of external electric field; the carrier scattering induced by photons and defects is rapidly amplified [19]. Hence, under this experimental condition, the mobility of the carriers exhibits only weak fluctuations with respect to the different external electric field's intensities. Correspondingly, according to Fig. S1 and Eq. (1), the carrier density is considered to be stable, similar to what happens in the presence of external electric fields with different intensities. For the MSM model, the current densities flowing through the reverse-biased Schottky barrier (J_r) and the forward-biased Schottky barrier (J_f) are given below [21]:

$$J_r = \frac{A^* T\sqrt{\pi E_{00}}}{k}\left\{q\left(V_1-\xi\right)+\frac{q\phi_1}{cosh^2\left(E_{00}/kT\right)}\right\}^{\frac{1}{2}} exp\left(-\frac{q\phi_1}{E_0}\right)\times exp\left[qV_1\left(\frac{1}{kT}-\frac{1}{E_0}\right)\right] \quad (3)$$

$$J_f = A^* T exp\left(-\frac{q\phi_2}{kT}\right)\times exp\left(-\frac{qV_2}{nkT}\right)\left[1-exp\left(-\frac{qV_2}{kT}\right)\right] \quad (4)$$

in which ϕ_1 and ϕ_2 are the effective heights of the two Schottky barriers respectively, n is an ideality factor, ξ is the distance from the Fermi level to the bottom of the conduction band, A^* is the Richardson constant of the semiconductor, and V_1 and V_2 are the applied bias voltages. The image force was included in the present model by regarding ϕ as an effective barrier. The constants E_0 and E_{00} are given by:

$$E_0 = E_{00}coth\left(\frac{E_{00}}{kT}\right) \quad (5)$$

$$E_{00} = \frac{\hbar q}{2}\left[\frac{N_d}{m^*\varepsilon_s\varepsilon_0}\right] \quad (6)$$

where m^* is the effective mass and N_d is the doping concentration. A well-known Matlab-based program PKUMSM is used for computing the numerical solutions of those equations by using Newton's method [21]. The basic parameters for describing the metal-semiconductor junction, such as the nanowire's conductivity, the two effective SBHs, and the carrier density, can be obtained.

Figure 4 shows the quantitative analysis of the relationship between the piezotronic related parameters and external electric field. The effective SBHs at the two electrodes are shown in Figs. 4(a) and 4(b) for different applied strains and external electric field's intensities. Here, taking the black lines as examples, these lines represent the results for the non-strained device. The lines indicate that both barrier heights decrease as the external electric field's intensity increases. The image force results in the SBH lowering, producing similarly reduced changing trend for different applied strains. At high electric field intensity, the barriers' heights decrease to 0.1 eV and the metal-semiconductor junctions become approximately Ohmic

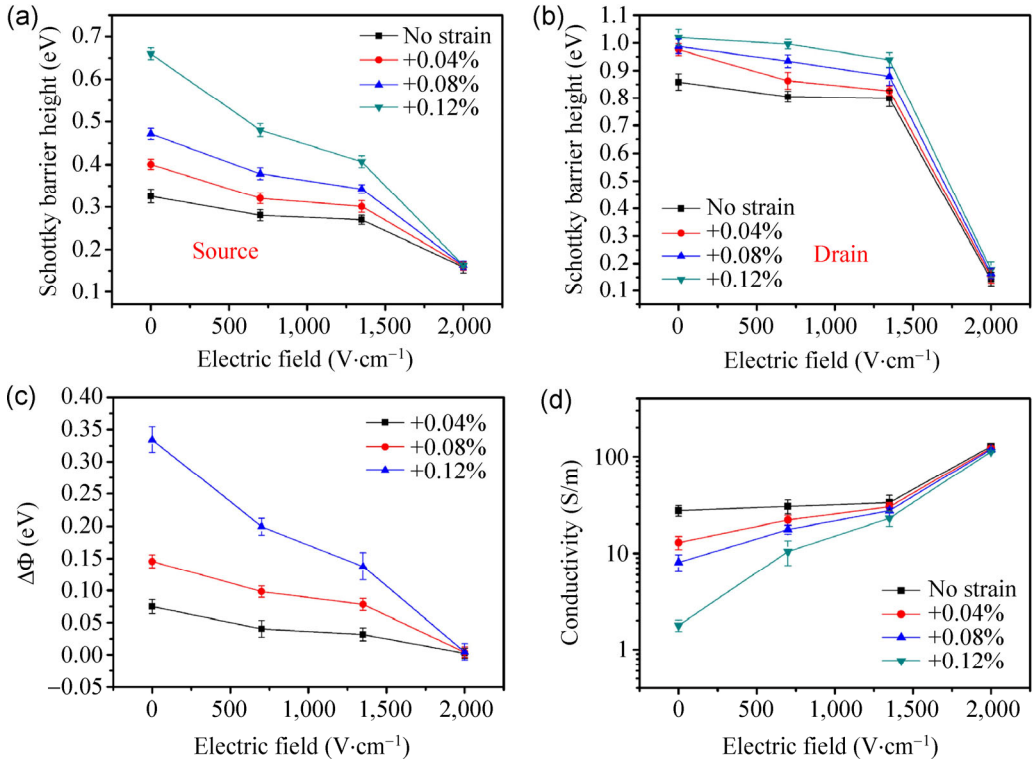

Figure 4 Quantitative descriptions of changes in the related parameters of low-conductivity nanowires, for different values of external electric field's intensity. (a), (b) Changes in SBHs at the source and drain electrodes, for different applied strains and external electric field's intensities. (c) Relative change in the barrier height ΔΦ on the source electrode. (d) Conductivity change as a function of external electric field's intensity.

contacts. Moreover, for one value of electric field's intensity, the barriers' heights increase with increasing tensile strain, which is modulated by the positive piezoelectric polarization charges; when the electric field's intensity increases, this modulation phenomenon is weakened. Actually, the change in the barriers' height is of principal concern, as it can be used for characterizing the carriers' transport modulation. As shown in Fig. 4(c), the change in the barriers' height decreases as the electric field's intensity increases for different tensile strains. It is clear that the strain-induced piezotronic response becomes weaker with increasing electric field's intensity. The conductivity of the device is also a function of external electric field's intensity for different applied strains, as shown in Fig. 4(d). For a fixed strain, the ZnO nanowire's conductivity increases simultaneously with increasing external electric field's intensity. This is because the image force contributes to the lowering of the barriers' height, resulting in more carriers that pass through the metal-semiconductor junction. It should be noted here that, owing to the modulation of the piezotronic effect, the varying trend is particularly distinctive for tensile strain of +0.12%. Moreover, the change in conductivity induced by tensile strain is smaller for stronger electric fields. Thus, the existing external electric field restrains the piezotronic response to influence the carrier transport at the metal-semiconductor junction. We attribute this inhibition of the piezotronic effect to the enhanced screening effect exerted by the external electric field on the positive piezoelectric polarization charges. As has been proposed in previous theoretical studies, the SBH change resulting from polarization charges can be expressed as [11]:

$$\Delta\phi = -\frac{q^2 \cdot \rho_{piezo} \cdot W_{piezo}^2}{2\varepsilon_s} \quad (7)$$

where ρ_{piezo} is the density of the effective polarization charges, ε_s is the semiconductor's permittivity (ZnO), W_{piezo} is the width of polarization charges distribution along the ZnO nanowire. Equation (7) indicates that the change of SBH is inversely proportional to the effective

polarization charges. Positive effective polarization charges attract the free electrons toward the metal-semiconductor interface and therefore decrease the SBH; negative effective polarization charges deplete the free electrons near the metal-semiconductor interface and therefore increase the SBH. As-synthesized ZnO micro/nanowires are naturally n-type doping and contain large numbers of free electrons. These free electrons screen some positive polarization charges in the depletion region. In addition, the external- electric-field induced lowering of SBH enables many more free electrons to flow through the depletion region, triggering the intensified screening effect on positive polarization charges. Hence, the piezotronic effect is more significant without external electric field, as illustrated in Figs. 3(a) to 3(c).

Figure 5 shows the *I*–*V* characteristics of devices belonging to the second group, with a moderate carrier density (about 1×10^{18} /cm^3). These devices exhibit typical non-symmetrical and Schottky properties for different applied tensile strains and different electric field's intensities. The current gradually decreases whether in the positive bias voltage range or the negative bias voltage range, when the tensile strain increases. For electric field's intensities reaching 1,350 V·cm^{-1}, the *I*–*V* curves become similar to straight lines and there is nearly no piezotronic response for different tensile strains. Figure 5(c) summarizes the relative change in currents at the two electrodes, derived from Figs. 5(a) and 5(b). Here, taking the black line as an example, the rate of the current change at the source electrode is not the same as that at the drain electrode. This non-symmetrical phenomenon confirms that the current change is mainly modulated by the piezotronic effect rather than by the piezoresistive effect, because the piezoresistive effect is a symmetrical effect while the piezotronic effect is not. The relevant effective barrier height values for different tensile strains at the two electrodes are shown in Fig. 5(d). The effective barrier heights increase as the tensile strain increases, and this trend becomes more significant in the absence of an electric field.

Devices with high carrier density (about 5×10^{18}/cm^3), belonging to the third group, are characterized in

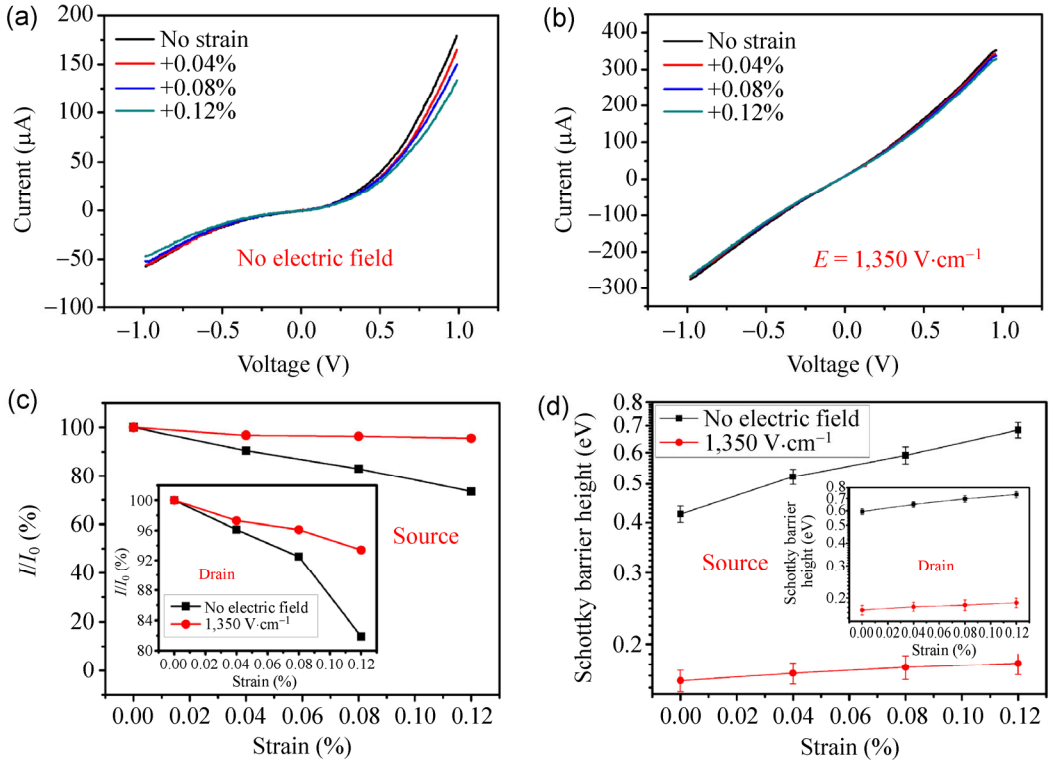

Figure 5 *I*–*V* curves for a moderate-conductivity device. Typical changes in transport characteristics for different applied strains and external electric field's intensities of (a) 0 V·cm^{-1} and (b) 1,350 V·cm^{-1}. The changes in current (c) and SBH (d) at the source and drain electrodes, for different applied strains and external electric field's intensities.

Fig. 6. The piezotronic response is not distinct compared with the first and second group devices, as shown in Fig. 6(a). At 700 V·cm^{-1}, the Schottky contact devices turned into Ohmic contact devices and there was no response to applied tensile strains. The relative current changes at the source and drain electrodes decreased with increasing tensile strain, as well as the data in Figs. 5(c) and 3(d). The effective barrier height remained at a nearly fixed value for two Schottky contacts without electric field. Devices with high carrier density can much easier become Ohmic contact devices with increasing electric field's intensity. The difference between the carrier densities in nanowires is inevitable during the synthesis of nanomaterials. However, a post-growth treatment can be applied for controlling the distribution range, such as treatment with oxygen plasma and annealing in oxygen. Finally, in Fig. 7(a), we present the noise current of the device without applied bias voltage, for different intensities of the electric field. The inset shows the current obtained when the device was not connected to the measurement system. The noise current changed slightly with external electric field's fluctuation and it was about 3 to 4 orders of magnitude smaller than the practically measured current, which could be ignored. Summary statistics regarding the number of devices transformed from Schottky contacts to Ohmic contacts at different external electric field's intensities and different doping levels are shown in Fig. 7(b).

4 Conclusions

In summary, we investigated the influence of external electric fields on the piezotronic effect, for external electric field's intensities ranging from 0 V·cm^{-1} to 2,000 V·cm^{-1}. After observing the piezotronic response, the typical behaviors could be divided into three groups, corresponding to devices with different conductivity, namely low, moderate, and high carrier densities of the ZnO nanowires used. For strong external electric fields, the piezotronic effect was significantly suppressed and the devices exhibited Ohmic contact behavior. We attribute this phenomenon to the image-force-induced lowering of SBH, which allowed many more

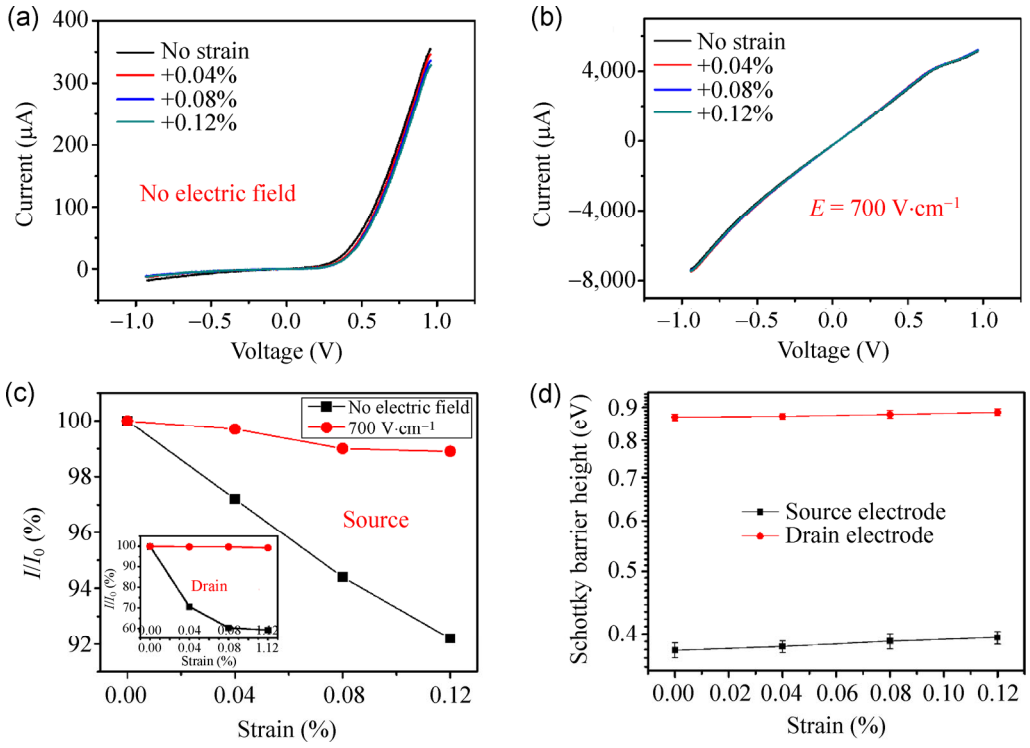

Figure 6 *I–V* curves for a high-conductivity device. Typical changes in transport characteristics for different applied strains and external electric field's intensities of (a) 0 V·cm^{-1} and (b) 700 V·cm^{-1}. (c) The change in current at the source and drain electrodes, for different applied strains and external electric field's intensities. (d) The change in SBH at the two electrodes, in the absence of external electric field.

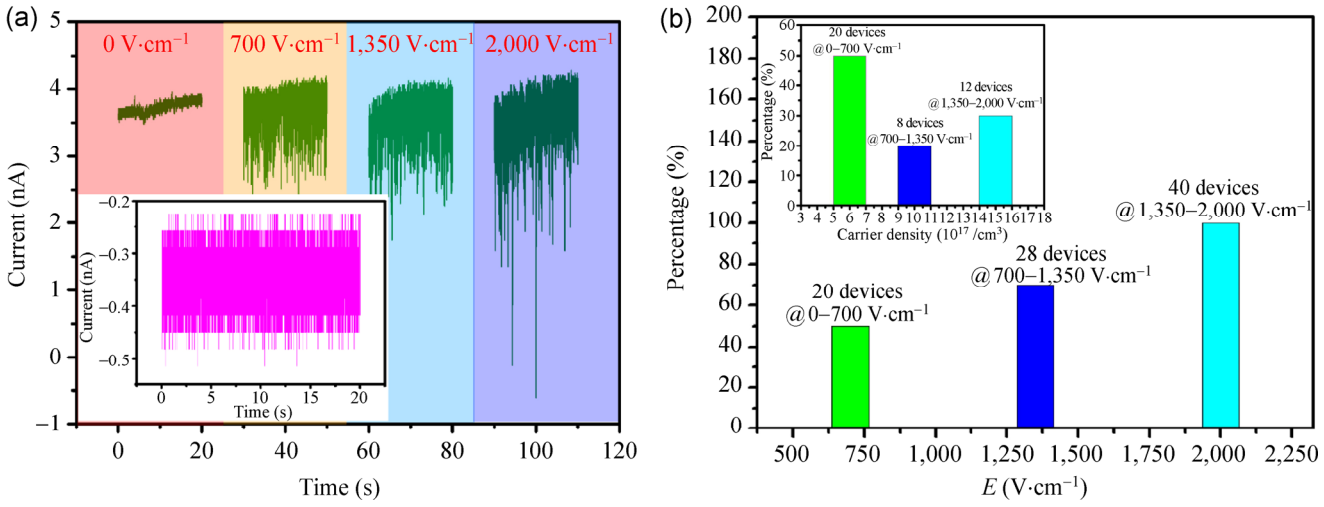

Figure 7 (a) The noise current of the device without applied bias voltage under different strength of electric field. The inset image is the noise current of the measuring system without connecting the device. (b) Statistical data when the device transformed from Schottky contact to Ohmic contact with different external electric field strength and different carrier density.

free carriers to pass through the metal-semiconductor interface and increase the screening effect on the positive piezoelectric polarization charges. This work will not only help us to better understand the fundamental mechanism of the piezotronic effect but may also assist in design and fabrication of piezotronic devices.

Acknowledgements

Research was supported by the "thousands talents" program for pioneer researcher and his innovation team, China, Beijing City Committee of science and technology (Z131100006013004, Z131100006013005).

Electronic Supplementary Material: Additional schematic figures on *I*–*V* curves of a device with Ohmic contact electrodes, for different external electric field's intensities without strains and *I*–*V* curves for different external electric field's intensities when the device was parallel to the substrate. This material is available in the online version of this article at http://dx.doi.org/10.1007/s12274-015-0749-3.

References

[1] Wang, Z. L. Nanopiezotronics. *Adv. Mater.* **2007**, *19*, 889–892.

[2] Wang, Z. L. The new field of nanopiezotronics. *Mater. Today* **2007**, *10*, 20–28.

[3] Zhou, J.; Gu, Y. D.; Fei, P.; Mai, W. J.; Gao, Y. F.; Yang, R. S.; Bao, G.; Wang, Z. L. Flexible piezotronic strain sensor. *Nano Lett.* **2008**, *8*, 3035–3040.

[4] Yang, Y.; Qi, J. J.; Gu, Y. S.; Wang, X. Q.; Zhang, Y. Piezotronic strain sensor based on single bridged ZnO wires. *Phys. Status Solidi RRL* **2009**, *3*, 269–271.

[5] Wang, X. D.; Zhou, J.; Song, J. H.; Liu, J.; Xu, N. S.; Wang, Z. L. Piezoelectric field effect transistor and nanoforce sensor based on a single ZnO nanowire. *Nano Lett.* **2006**, *6*, 2768–2772.

[6] Wu, W. Z.; Wen, X. N.; Wang, Z. L. Taxel-addressable matrix of vertical-nanowire piezotronic transistors for active and adaptive tactile imaging. *Science* **2013**, *340*, 952–957.

[7] Pan, C. F.; Dong, L.; Zhu, G.; Niu, S. M.; Yu, R. M.; Yang, Q.; Liu, Y.; Wang, Z. L. High-resolution electroluminescent imaging of pressure distribution using a piezoelectric nanowire LED array. *Nat. Photonics* **2013**, *7*, 752–758.

[8] Wen, X. N.; Wu, W. Z.; Wang, Z. L. Effective piezo-phototronic enhancement of solar cell performance by tuning material properties. *Nano Energy* **2013**, *6*, 1093–1100.

[9] Zhang, Z.; Liao, Q. L.; Yu, Y. H.; Wang, X. D.; Zhang, Y. Enhanced photoresponse of ZnO nanorods-based self-powered photodetector by piezotronic interface engineering. *Nano Energy* **2014**, *9*, 237–244.

[10] Xue, F.; Zhang, L. M.; Tang, W.; Zhang, C.; Du, W. M.; Wang, Z. L. Piezotronic effect on ZnO nanowire film based temperature sensor. *ACS Appl. Mater. Interfaces* **2014**, *6*, 5955–5961.

[11] Zhang, Y.; Liu, Y.; Wang, Z. L. Fundamental theory of piezotronics. *Adv. Mater.* **2011**, *23*, 3004–3013.

[12] Hu, Y. F.; Klein, B. D. B.; Su, Y. J.; Niu, S. M.; Liu, Y.; Wang, Z. L. Temperature dependence of the piezotronic effect in ZnO nanowires. *Nano Lett.* **2013**, *13*, 5026–5032.

[13] Yang, S. Z.; Wang, L. F.; Tian, X. Z.; Xu, Z.; Wang, W. L.; Bai, X. D.; Wang, E. G. The piezotronic effect of zinc oxide nanowires studied by in situ TEM. *Adv. Mater.* **2012**, *24*, 4676–4682.

[14] Shi, J.; Starr, M. B.; Wang, X. D. Band structure engineering at heterojunction interfaces via the piezotronic effect. *Adv. Mater.* **2012**, *24*, 4683–4691.

[15] Zhang, Y.; Yan, X. Q.; Yang, Y.; Huang, Y. H.; Liao, Q. L.; Qi, J. J. Scanning probe study on the piezotronic effect in ZnO nanomaterials and nanodevices. *Adv. Mater.* **2012**, *24*, 4647–4655.

[16] Xu, S. G.; Guo, W. H.; Du, S. W.; Loy, M. M. T.; Wang, N. Piezotronic effects on the optical properties of ZnO nanowires. *Nano Lett.* **2012**, *12*, 5802–5807.

[17] Geng, C. Y.; Jiang, Y.; Yao, Y.; Meng, X. M.; Zapien, J. A.; Lee, C. S.; Lifshitz, Y.; Lee, S. T. Well-aligned ZnO nanowire arrays fabricated on silicon substrates. *Adv. Funct. Mater.* **2004**, *14*, 589–594.

[18] Yang, P. D.; Yan, H. Q.; Mao, S.; Russo, R.; Johnson, J.; Saykally, R.; Morris, N.; Pham, J.; He, R. R.; Choi, H. J. Controlled growth of ZnO nanowires and their optical properties. *Adv. Funct. Mater.* **2002**, *12*, 323–331.

[19] Sze, S. M. *Physics of Semiconductor Devices, 2nd ed.;* Wiley: New York, 1981.

[20] Zhang, Y.; Hu, Y. F.; Xiang, S.; Wang, Z. L. Effects of piezopotential spatial distribution on local contact dictated transport property of ZnO micro/nanowires. *Appl. Phys. Lett.* **2010**, *97*, 033509.

[21] Liu, Y.; Zhang, Z. Y.; Hu, Y. F.; Jin, C. H.; Peng, L. M. Quantitative fitting of nonlinear current–voltage curves and parameter retrieval of semiconducting nanowire, nanotube and nanoribbon devices. *J. Nanosci. Nanotechnol.* **2008**, *8*, 252–258.

[22] Zhang, Z. Y.; Yao, K.; Liu, Y.; Jin, C. H.; Liang, X. L.; Chen, Q.; Peng, L. M. Quantitative analysis of current–voltage characteristics of semiconducting nanowires: Decoupling of contact effects. *Adv. Funct. Mater.* **2007**, *17*, 2478–2489.